Mathematical Biosciences and Engineering

MBE, 19(9): 9321–9334.
DOI: 10.3934/mbe.2022433
Received: 04 April 2022
Revised: 17 May 2022
Accepted: 25 May 2022
Published: 24 June 2022

http://www.aimspress.com/journal/MBE

Research article

A combined functional dorsal nerve model of the foot

Muhammad Z. Ul Haque[1,2,*], Peng Du[2] and Leo K. Cheng[2]

[1] Department of Biomedical Engineering, Salim Habib University, Karachi, Pakistan
[2] Auckland Bioengineering Institute, University of Auckland, Auckland, New Zealand

* **Correspondence:** Email: muhammad.zeeshan@shu.edu.pk.

Abstract: The nerves in the skin surface of the foot are comprised of unmyelinated smaller somatic nerves and larger myelinated sensory nerves. Current diagnostic methods are unable to evaluate combined nerve conduction velocity (NCV) from both unmyelinated smaller somatic nerve (USSN) and myelinated larger nerves (MLN) respectively. Computational models may provide an alternative tool to determine the NCV of the combined nerve. Therefore, a combined functional dorsal nerve model (CFDNM) of the various dorsal nerves along with its associated nerve ending of the human foot is proposed and constructed. The combined dorsal nerve model consists of synthetic USSN (SUSSN) and dorsal MLN of the foot. The unmyelinated as well as myelinated electrophysiological nerve models were used to simulate selected SUSSN and MLN of the foot by injecting an external stimulus at the most distal part of SUSSN of the foot through the use of bidomain model. Results from our work demonstrated that the action potential propagated from the most distal part to proximal part of distinct dorsal nerves of the foot, e.g., the simulated NCV of the combined intermediate dorsal cutaneous nerve (IDCN) of the foot was 28.4 m s^{-1}. The CFDNM will provide a vital tool for diagnosis initially small fibre neuropathy (SFN) by computing NCV in the prospective studies.

Keywords: myelinated sensory nerve; unmyelinated somatic nerve; nerve conduction velocity; computational model; electrophysiological nerve model; action potential; small fibre neuropathy

1. Introduction

The nerves of the foot are comprised of both unmyelinated and myelinated nerves [1–3]. The plantar and dorsal side of the foot is composed of several sensory and motor nerves in concert with unmyelinated somatic nerves that are present in the skin surface of the foot. Afferent fibres innervating

the skin of the foot convey information to the central nervous system which is necessary to control body mechanics and accurate loading [4,5]. Furthermore, examining nerve function in the foot can be beneficial for diagnosis of various types of diabetic mellitus conditions such as diabetic neuropathy and non-healing ulcers of the foot [6,7].

The examination, as well as recognition of diabetic neuropathy is an intricate process [8,9]. Clinically a number of different diagnostic methods have been employed to diagnose small and larger fibre diabetic neuropathy. For instance, sensory nerve conduction studies (NCS) is useful for computing nerve conduction velocity (NCV) along the entire length of larger peripheral nerve rather than determination of the patient-specific nerve damage response [10,11]. Skin biopsies are employed for the examination of small fibre neuropathy (SFN) by quantifying a decrease in intra-epidermal nerve fibre density (IENFD) [12,13]. Although, the aforementioned methods have been successfully applied clinically, unfortunately, there is no diagnostic method that examines the combined effect of USSN and MLN present in the skin.

Moreover, some of the problems related to these diagnostic methods remains unsolved, the position of the electrodes to measure the specific nerve response in the combined nerve, actual NCV in the specific nerve location, length of the nerves is unknown in combined nerves and no electrical stimulation procedure is available to measure NCV in USSN. Hence, computational modelling of the nerves in the foot is likely to demonstrate a beneficial tool for the examination and prognosis of combined nerve damage response without dependence on human or animal experimental studies in diabetic neuropathy.

There are a number of existing computational models of the upper and lower limbs, e.g., 3D human medial nerve model [14], model of the nerves in the lower limb used for assessing functional electrical stimulation [15], model for lower limb sensorimotor neuroprostheses [16], human model for investigating the performance of feet in balance [17], model of the foot for assessing soft tissue stiffening in the foot [18], model for the examination of blood transport in the foot [19], perturbed nerve geometrical model of the foot for the simulation of SFN [20]. However, there is no known computational models which specifically determines the NCV in the combined USSN and MLN of the human foot. Also, in our previous study, an initial framework was proposed for the construction of one-dimensional (1D) synthetic single element structural and functional model characterizing the anatomical and physiological performance of the foot nerves [21], but it was not used to simulate the action potential in the combined nerve model.

Therefore, in this study, a baseline combined functional, i.e., synthetic unmyelinated smaller somatic nerves (SUSSN) and myelinated larger nerves (MLN) model is proposed. The proposed model was then used to compute the combined NCV in the various larger dorsal nerves of the foot by applying an extracellular stimulus current at the most distal point of the selected SUSSN using unmyelinated and myelinated electrophysiological nerve model. A grid based finite difference method was employed to solve the bidomain conduction model. The developed combined functional model will be utilized in prospective studies for the examination of the combined response of small as well as large fibre neuropathy by examining the NCV in the desired nerve.

2. Materials and methods

In this research work, a combined one dimensional (1D) functional model of various dorsal nerves in the human foot is proposed and constructed. The combined functional dorsal nerve model (CFDNM)

incorporates the modified unmyelinated Hodgkin-Huxley (UHH) [22] and the myelinated Chiu, Ritchie, Rogert, Stagg and Sweeney (MCRRSS) [23] electrophysiological nerve models. These models were employed to construct and propagate action potential using grid based finite difference method to obtain the Bidomain model solution in SUSSN and MLN respectively. The simulation studies in CFDNM were performed on a single nerve fibre (SNF) of the selected SUSSN and MLN nerve. SNF in the various dorsal nerves of the CFDNM was selected in order to achieve the optimal NCV for a diameter of 1.5 and 10 μm in the selected SUSSN and MLN as evident from previous studies [24,25] respectively. The components incorporated in the construction of the CFDNM are presented in Figure 1.

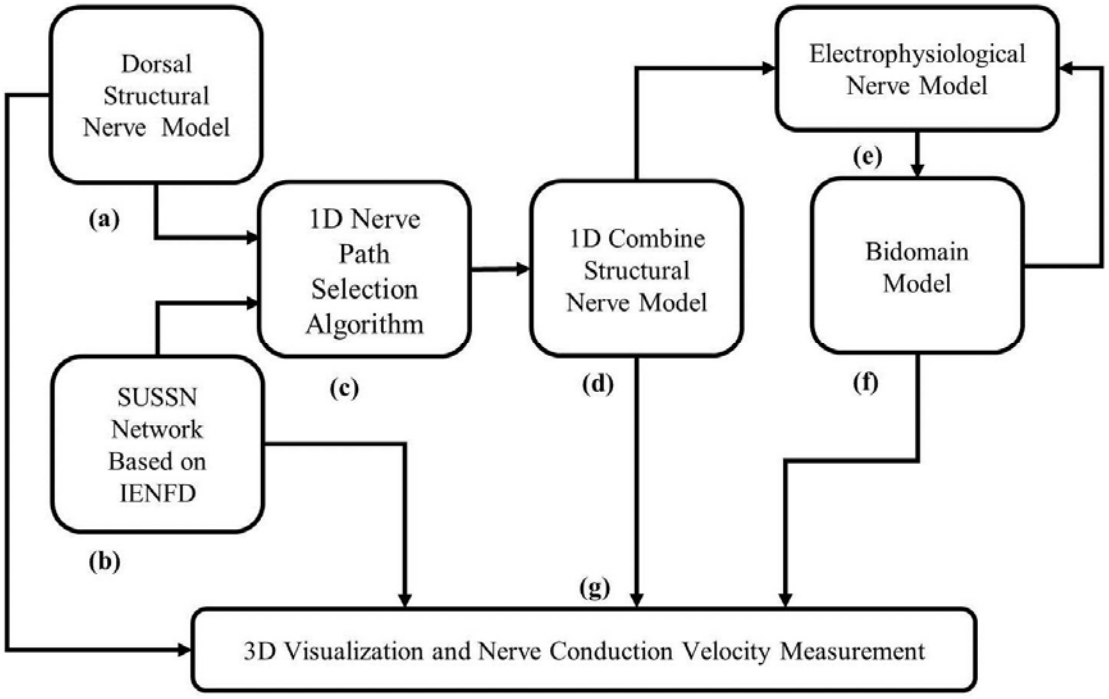

Figure 1. Phases incorporated in the construction of the CFDNM. (a) Construction of larger dorsal structural nerve model (DSNM) using 1D cubic Hermite basis function, (b) Construction of SUSSN network based on intra-epidermal nerve fibre density (IENFD) as well as Monte Carlo's Algorithm, (c) Development of 1D nerve path selection algorithm (NPSA) to select a single 1D SUSSN region and their connected MLN path from the respective DSNM model respectively, (d) Combined 1D selected nerve structural model includes selected SUSSN path along with their connected MLN path, (e) CellML based UHH and MCRRSS nerve models used for action potential generation in the combined structural nerve model respectively, (f) Bidomain model for action potential generation and propagation along the 1D combined nerve model, and (g) 3D visualization of 1D combined nerve structural model and NCV measurement of the selected 1D combined nerve model.

2.1. 1D combined dorsal structural nerve model (DSNM)

Initially, the dorsal structural nerve model (DSNM) consisting of various dorsal nerves of the foot

was constructed from the image digitization of anatomical illustrations using 1D cubic Hermite basis function as described in detail previously [26]. This DSNM was used as input for the development of CFDNM as shown in Figure 1(a). The second stage for the development of 1D combine DSNM was to construct the normal bifurcated synthetic somatic intra-epidermal nerve fibre (IENF) network from one of the cutaneous branch of the larger DSNM over the complete region of foot as discussed in previous studies [26,27] and mentioned in Figure 1(b). The previously constructed normal synthetic IENF model was based on quantitative data of IENFD at different areas of the foot and modifying the previously used Monte-Carlo algorithm [27]. The selected SUSSN network was again selected as an input for the CFDNM construction. Since, the developed DSNM incorporates different MLN branches along with their cutaneous branches and the SUSSN network over the entire skin of the foot. Also, standard NCS only executed on 20% of the distinct largest diameter [10,11]. Hence, a 1D tree nerve path selection algorithm (NPSA) was also constructed as represented in Figure 1(c), which automatically selected the 1D nerve path from the desired nerve ending point by checking the shortest path between the starting and target nodes. This was done by choosing the most distal nerve point of the selected nerve mesh as the beginning nerve point whereas the most proximal nerve points of the selected larger nerve mesh acted as target nerve points using aforementioned 1D NPSA. The combined 1D DSNM was then developed by combining the selected 1D SUSSN path (present in the foot's skin) along with their connected MLN using a 1D cubic Hermite Basis function as mentioned in Figure 1(d).

2.2. 1D combined functional dorsal nerve model (CFDNM)

The 1D combined DSNM was implemented as an input for the development of CFDNM. For this purpose, the UHH and MCRRSS nerve models encoded in CellML [28,29] were used to simulate action potential propagation in the SNF of 1D combined structural nerve model, i.e., desired SUSSN of the foot's skin and interconnected dorsal MLN as illustrated in Figure 1(e) respectively. These electrophysiological nerve models were utilized to determine action potential in a single grid point of the desired SUSSN of the skin of the foot and interconnected dorsal MLN respectively. Equations (1) and (2) are the mathematical equations and their parameters employed in both UHH [22] and MCRRSS [23], implemented in CellML.

Unmyelinated HH model

$$\frac{dV_{SUSSN}}{dT} = \frac{I_{StSUSSN} - (I_{NaSUSSN} + I_{KSUSSN} + I_{LSUSSN})}{C_{SUSSN}} \tag{1}$$

where, $I_{StSUSSN}$ is an external stimulus current required to activate the membrane of selected SUSSN and stimulus current value is 0.7 μA with duration of 0.5 ms, $C_{SUSS,N}$ is the membrane capacitance with a value of 0.1 μF mm^{-2}, $\frac{dV_{SUSSN}}{dT}$ indicates membrane potential value in a specified time of SUSSN, $I_{NaSUSSN}$ represents the depolarization of the cell, I_{KSUSSN} and I_{LSUSSN} are responsible for the repolarization of the cell.

Myelinated CRRSS Model

$$\frac{dV_{MLN}}{dT} = \frac{\frac{I_{stMLN}}{\pi D_{MLN} L_{MLN}} - I_{NaMLN} + I_{LMLN}}{C_{MLN}} \tag{2}$$

where, I_{stMLN} is the stimulus current used in CRRSS model, C_{MLN} is the membrane capacitance of CRRSS model having 0.1 μF mm^{-2}, $\frac{dV_{MLN}}{dT}$ represents the membrane potential in a specified time of MLN, I_{NaMLN} and I_{LMLN} are the ionic currents of the sodium and leakage channel used in MLN, D_{MLN} represents the diameter of the nerve with a value of 1.3 mm, L_{MLN} indicates nodal gap length having 7 μm in length.

The 1D combined DSNM was employed as a contribution for the action potential propagation along the SNF of the 1D combined nerve model. Subsequently, the nerve mesh was divided into equally space grid point along the whole length of 1D combined selected nerve model. The bidomain model was utilized to simulate the action potential generation and propagation along the complete path of 1D selected combined nerve mesh by injecting an extracellular current in the most distal part of the 1D path SUSSN as shown in Figure 2(g). The CellML based electrophysiological nerve models and bidomain model formed a feedback loop for computing updated action potential, the ionic currents, and their particular ODEs values at each grid point repeatedly until it reached a final desired time period. For this purpose, grid based finite difference method and Euler numerical integration technique for implicitly solving differential equations of the UHH and MCRRSS models' ionic currents respectively.

2.3. 3D visualization and computation of NCV

Continuum mechanics graphical user interface (CMGUI), a front end part of CMISS (https://www.cmiss.org) [30] was used to visualise the 3D image of the combine DSNM and also the action potential propagation from the most distal part of the selected SUSSN to the proximal side of the connected 1D MLN. The NCV was computed by dividing the total distance of the specific 1D combined SUSSN connected with the MLN over time to propagate the action potential from the distal part to the proximal part.

3. Results

The combined 1D structural dorsal nerve model of the foot was constructed which encompasses both the SUSSN and MLN. As an example, the selection of the 1D nerve path from one of the SUSSN network and their connected larger dorsal IDCN using 1D nerve selection algorithm is presented in Figure 2. The dorsal nerve model was comprised of a number of nerves as shown in Figure 2(a) and illustrated by the black line with the node points represented by the red spheres. The desired selected 1D IDCN path using abovementioned 1D NPSA is illustrated in Figure 2(b) by the blue line with the red spheres. Figure 2(c) represented the combined larger dorsal nerve model (black line) as well as selected 1D IDCN path (blue line) using 1D NPSA respectively. The synthetic IENF network from the cutaneous branch at the fourth dorsal toe is shown by black lines with the node points represented by the red sphere as shown in Figure 2(d). The beginning node point was selected randomly as the most distal nerve ending point of this selected IENF network. The selected smaller 1D nerve path using the algorithm is given in Figure 2(e) and represented by the blue line with the red sphere. The combined IENF network and the selected 1D larger nerve path from this chosen IENF network is shown in Figure 2(f). Finally, the larger 1D IDCN nerve path and the selected 1D IENF network path are combined to construct 1D IDCN mesh using the 1D cubic Hermite basis function explained in

Figure 2(g) and represented by blue line and dorsal structural nerve model represented by black line respectively.

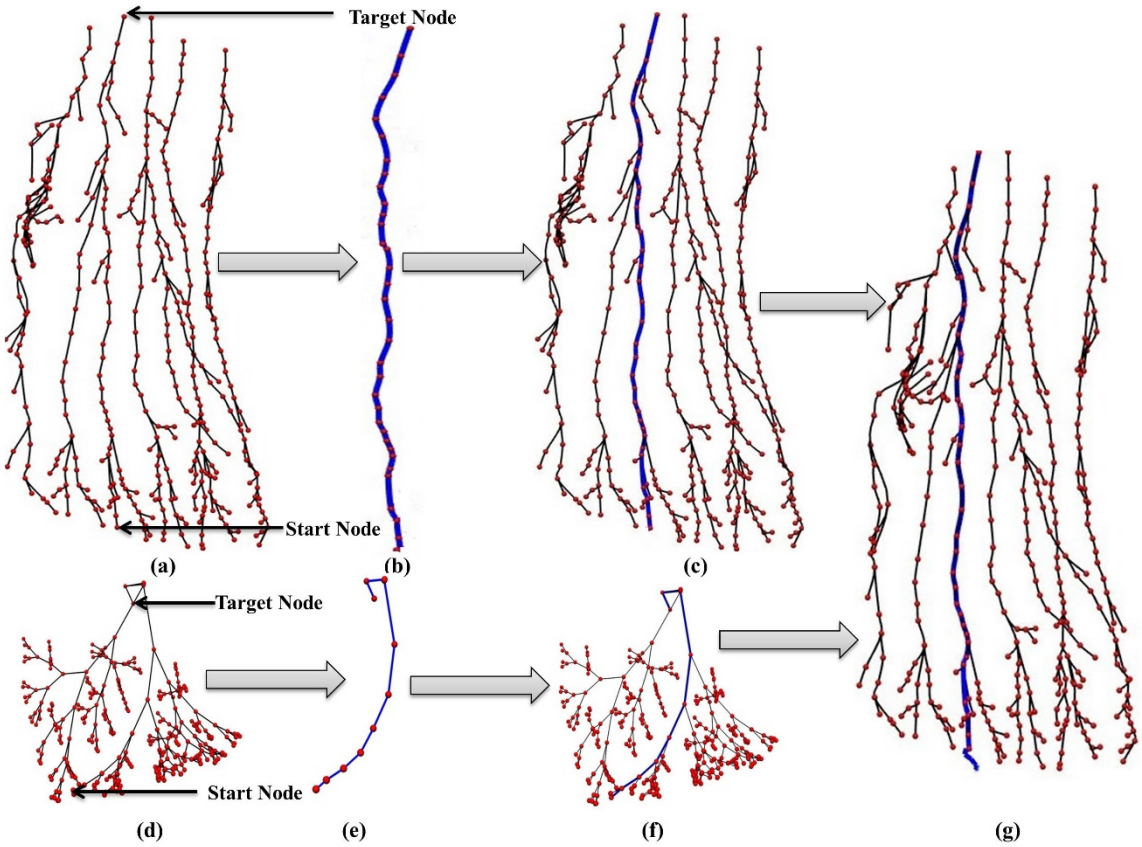

Figure 2. Selection of 1D larger and smaller nerve paths from the developed dorsal structural nerve model of the foot using 1D path algorithm: (a) Normal dorsal nerve model, (b) Selection of the 1D IDCN path from the dorsal nerve model, (c) Selected 1D IDCN nerve with a dorsal nerve model, (d) Synthetic IENF network at the fourth dorsal toe, (e) 1D smaller nerve selection from the IENF network, (f) Selected 1D nerve path along with synthetic IENF network at fourth toe, (g) Combined selected 1D nerve path consists of larger and smaller nerve.

For simulation studies in the developed combined 1D nerve model, initially single MLN diameter, e.g., IDCN along with associated 1D SUSSN endings (present in the fourth toe's region) was selected as shown in Figure 2(g) as an input. Consequently, an extracellular stimulus current was injected at the most distal part of selected SNF of IDCN for determining the NCV. The intensity of this stimulus current was 0.7 μA with duration of 0.5 ms with an initial stimulus time of 1 ms. The diameter of distal SUSSN endings was 1.5 μm since it provided the maximum NCV [31]. The diameter of the SNF myelinated IDCN was set at 10 μm as diameter of each single MLN of human nerve varies between 6–10 μm [32]. An assumption was that diameter of 1D combined selected SNF IDCN remains same over the complete passage of the nerve. The intracellular and extracellular conductivities of the selected SUSSN and MLN IDCN were 32.5 and 34.5 mS μm^{-1} respectively. Once the simulation studies were completed on the selected IDCN along with the most distal smaller somatic nerves connected with the cutaneous branch of IDCN, then the simulation studies were performed on each of

the larger dorsal nerves along with most distal single SUSSN associated with the cutaneous branch of dorsal MLN. The parameters that were used to simulate the different nerves present in the 1D CFDNM are presented in Table 1.

Table 1. Simulation parameters employed in CFDNM of the human foot.

Dorsal nerves in the foot	Parameters and their values used for the simulation			
	Nerve types	Length of the nerve (mm)	Intracellular conductivity (mS μm^{-1})	Extracellular conductivity (mS μm^{-1})
Medial dorsal cutaneous nerve (MDCN)	Larger	248.2	35.0	35.0
	Smaller	19.1	32.0	32.0
Intermediate dorsal cutaneous nerve (IDCN)	Larger	232.1	34.5	34.5
	Smaller	12.4	32.5	32.5
Deep peroneal nerve (DPN)	Larger	237.8	37.0	37.0
	Smaller	14.1	35.0	35.0
Sural nerve (SN)	Larger	260.9	25.0	25.0
	Smaller	9.1	75.0	75.0
Lateral dorsal cutaneous nerve (LDCN)	Larger	99.9	62.5	62.5
	Smaller	27.4	50.0	50.0
Saphenous nerve (SaN)	Larger	165.1	35.0	35.0
	Smaller	25.8	32.0	32.0

The action potential propagation in the larger MLN of IDCN along with their connected SUSSN is represented in Figure 3. The orthodromic NCS simulation studies were opted in this work, i.e., the action potential propagated from each of the very distal smaller nerves through the larger IDCN and travelled towards the very proximal end of the nerve fibres. Figure 3(a) illustrated the combined 1D CFDNM and selected combined 1D SUSSN and MLN IDCN nerve model with no action potential at 0.1 ms. Figure 3(b) represented that action potential was propagated at four different locations and time periods in the 1D larger combined IDCN nerve model, when an external current was applied at the most distal part of SUSSN using bidomain model.

Additionally, the NCV in the SNF of the combined functional IDCN nerve model was determined by measuring the total length of the selected 1D combined IDCN nerve (consists of both SUSSN and MLN IDCN) and dividing by the time at which action potential propagated from the distal part of SUSSN endings of IDCN to the proximal part of the MLN. The simulated total length of the combined IDCN model was 244.5 mm and the simulated onset and peak latency were 8.6 and 8.9 ms respectively.

Similarly, the NCV in the SNF of the other combined larger dorsal nerve were simulated by altering the intracellular and the extracellular conductivities of the MLN and SUSSN. The simulated combined onset and peak latencies and NCV in the SNF of various larger dorsal nerves of the combined nerve model is presented in Figure 4.

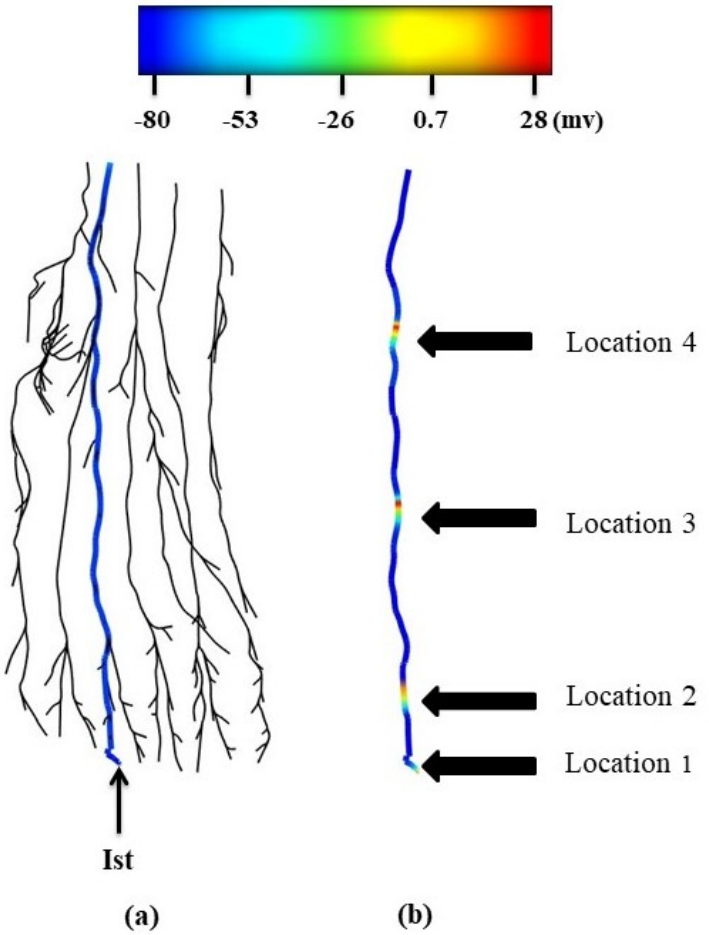

Figure 3. Action potential propagation in the CFDNM: (a) Depiction of CFDNM (black lines) and the selection of 1D larger combined IDCN nerve model (blue lines) with no action potential at 0.1 ms. (b) Propagation of action potential in the combined functional 1D IDCN nerve model at location 1 (2 ms), location 2 (4 ms), location 3 (6 ms) and location 4 (8 ms) respectively.

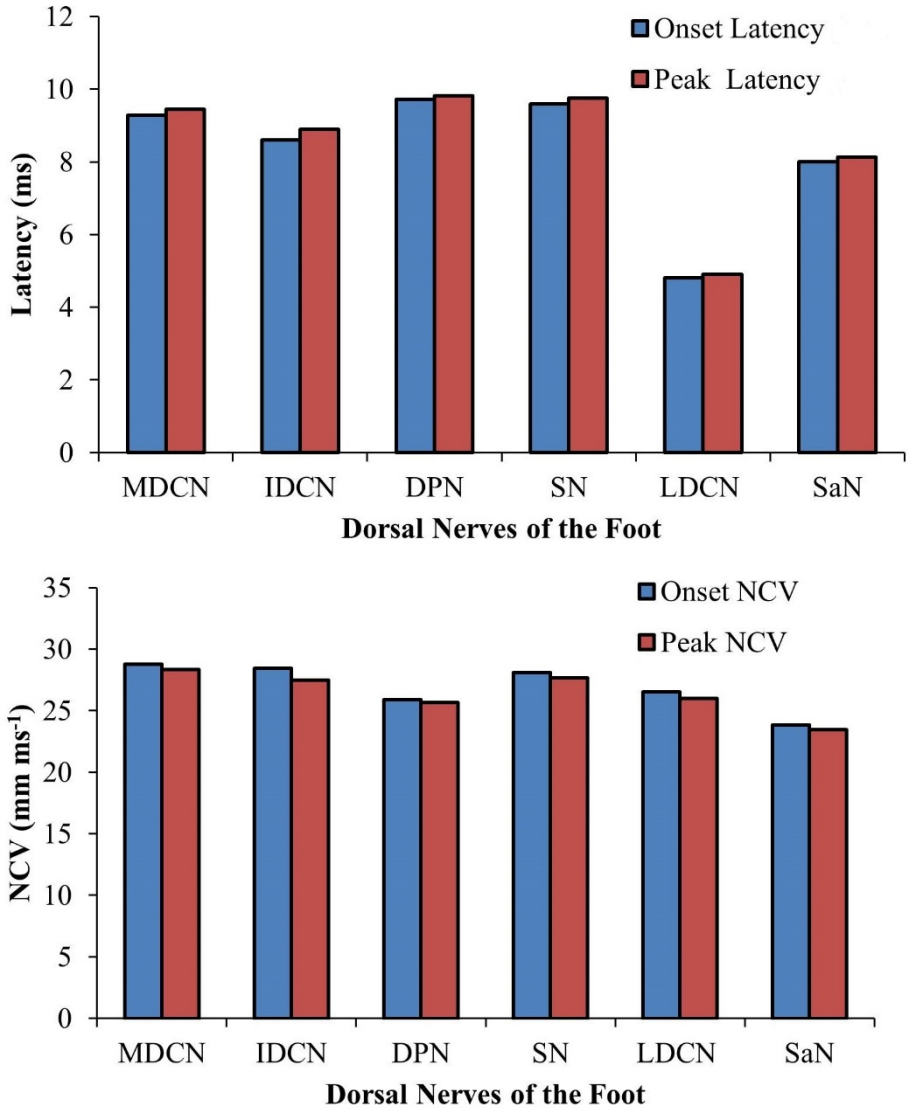

Figure 4. Latencies and nerve conduction velocities (NCV) in the SNF of various nerves of the CFDNM of the foot.

4. Discussion

In this study, a baseline CFDNM of the human foot was proposed and developed. Initially, the combined DSNM was developed and it comprised of selected SUSSN endings selected along with their connected MLN from the dorsal nerve model respectively. The CFDNM was then constructed by implementing the modified UHH and MCRRSS nerve models to simulate the electrical activity in the SUSSN and its connected MLN, primarily in larger IDCN and the synthetic somatic nerve present in the second dorsal toe by injecting an extracellular stimulus current at the most distal part of the selected SUSSN endings.

The intracellular and the extracellular conductivities in the CFDNM were higher as compared to the relevant larger nerve of the foot (see Table 1). This was done to achieve the appropriate NCV of this combined nerve closely matched with the NCV of the same larger nerve model. For instance, the

NCV in the combined 1D IDCN model was 28.4 m s^{-1} as compared to experimental NCV of larger IDCN were ranges between 33–53 m s^{-1} [33] as the diameter of the nerve is proportional to NCV [34]. Secondly, in this study the experimental based maximum diameter of the SNF of the larger nerve and USSN were employed to achieve the maximum NCV respectively [24,25]. Therefore, the developed combined 1D baseline nerve model was useful in determining a suitable NCV of any specific dorsal nerve location with a variable length of nerve by changing the diameter and conductivity values respectively. This was especially beneficial because NCS and skin biopsy are only limited to the larger and smaller nerves clinically [10–13].

There were some limitations with the combined baseline 1D functional nerve models. The first limitation of this model was with the 1D NPSA. This algorithm was not able to automatically select 2-3 SUSSN endings into a single nerve ending points coming from a specific cutaneous nerve branch of a MLN. The selection of 2-3 nerve endings was necessary for simulating and diagnosing diabetic foot ulceration as the SUSSN endings were very close with each other. Eventually, the combined model was not able to perform simulation studies with an automatic selection of 2-3 nerve endings points although simulation studies with the single nerve ending were giving comparable NCV with the related larger nerve NCV.

Future investigation should be conducted to address the current model limitations. The 1D NPSA can be further improved by connecting multiple nerves endings to one nerve point by defining the shortest path between two nerve points in the selected nerve endings. Finally, once the multiple, 2-3 nerve endings were selected automatically from the 1D NPSA; these selected nerve endings were stimulated by with an extracellular stimulus current. The desired compound NCV was obtained by assigning the suitable intracellular and the extracellular conductivities to each of the nerve endings.

Moreover, the developed baseline CFDNM will be modified to simulate the functional outcomes by computing NCV in distal sensory neuropathy (DSN), a common and painful sensory symptom of diabetes mellitus [35,36]. Previous researches suggested that axonal degeneration is the most common problem occurs in DSN patients [35–39]. Therefore, perturbation studies in the developed CFDNM may be perform to investigate DSN by degenerating axons in SNF of SUSSN and the distal part of the MLN as most of the nerve was damaged distally [40]. These axonal degenerations in the SNF of the selected nerve of the CFDNM were achieved by varying the length of the perturbed SUSSN and MLN, lowering the intracellular and extracellular conductivities respectively, while the conductivities in the remaining normal MLN remains constant. All other parameter values, e.g., diameter of the selected SUSSN and MLN, stimulus current etc. will be kept constant as of normal baseline CFDNM. In this way, the functionally interrupted CFDNM will be employed for the examination and diagnosis of diabetic neuropathy in early stages.

Furthermore, the CFDNM will be validated in the forthcoming study by performing experimental NCS studies and considering demographic data of the normal and diabetic neuropathic subject using the following data collection:

1) Determine the subject specific diameters of SUSSN and MLN.
2) Apply the realistic stimulus current and stimulus duration in the developed CFDNM.
3) Identify and determine the realistic location and distance of stimulating and recording electrodes in a normal and diabetic neuropathy patient.
4) Compute and validate the NCV of the various SUSSN and MLN in CFDNM with the experimental NCS.

5. Conclusions

The first computational combined functional dorsal nerve model (CFDNM) was developed. The CFDNM was able to determine and compare the sensory NCV in the various normal combined dorsal nerves of the foot. These models were next used to investigate the functional consequences of combined nerves in various locations of the foot by determining the NCV and SNAP for diagnosing different diabetic neuropathy conditions such as diabetic foot ulceration in its initial phase.

Acknowledgments

The authors would like to gratitude New Economy Research of New Zealand and Auckland Bioengineering Institute for providing their support in accomplishment of this research work. Additionally, the authors would like to thank Drs. Marc Jacobs and Justin Fernandez for their help in carrying out the current research work.

Conflict of interest

The authors declare that there is no conflict of interest.

References

1. H. Ellis, The nerves of the leg and foot, *Anaesth. Intensive Care Med.*, **11** (2010), 95–97. https://doi.org/10.1016/j.mpaic.2009.12.007
2. T. Arakawa, S. Sekiya, K. Kumaki, T. Terashima, Ramification pattern of the deep branch of the lateral plantar nerve in the human foot, *Ann. Anat. Anat. Anz.*, **187** (2005), 287–296. https://doi.org/10.1016/j.aanat.2005.02.009
3. S. Bianchi, C. Martinoli, Foot, in *Ultrasound of The Musculoskeletal System*, Medical Radiology, Springer, Berlin, Heidelberg, (2007), 835–888. https://doi.org/10.1007/978-3-540-28163-4_17
4. L. Ren, Z. Qian, L. Ren, Biomechanics of musculoskeletal system and its biomimetic implications: A review, *J. Bionic Eng.*, **11** (2014), 159–175. https://doi.org/10.1016/S1672-6529(14)60033-0
5. P. M. Kennedy, J. T. Inglis, Distribution and behaviour of glabrous cutaneous receptors in the human foot sole, *J. Physiol.*, **53** (2002), 995–1002. https://dx.doi.org/10.1113%2Fjphysiol.2001.013087
6. M. Edmonds, C. Manu, P. Vas, The current burden of diabetic foot disease, *J. Clin. Orthop. Trauma*, **17** (2021), 88–93. https://doi.org/10.1016/j.jcot.2021.01.017
7. P. R. J. Vas, J. Lucas, S. Arshad, M. E. Edmonds, Neuropathic diabetic foot ulceration, in *Limb Salvage of the Diabetic Foot*, Springer, Cham, (2019), 53–76. https://doi.org/10.1007/978-3-319-17918-6_4
8. Z. Iqbal, S. Azmi, R. Yadav, M. Ferdousi, M. Kumar, D. J. Cuthbertson, et al., Diabetic peripheral neuropathy: epidemiology, diagnosis, and pharmacotherapy, *Clin. Ther.*, **40** (2018), 828–849. https://doi.org/10.1016/j.clinthera.2018.04.001
9. K. N. Lew, T. Arnold, C. Cantelmo, F. Jacque, H. Posada-Quintero, P. Luthra, et al., Diabetes distal peripheral neuropathy: Subtypes and diagnostic and screening technologies, *J. Diabetes Sci. Technol.*, **16** (2022), 295–320. https://doi.org/10.1177%2F19322968211035375

10. S. W. Ahn, B. N. Yoon, J. E. Kim, J. M. Seok, K. K. Kim, Y. M. Lim, et al., Nerve conduction studies: basic principal and clinical usefulness, *Ann. Clin. Neurophysiol.*, **20** (2018), 71–78. https://doi.org/10.14253/acn.2018.20.2.71
11. J. R. Daube, D. I. Rubin, Nerve conduction studies, in *Aminoff's Electrodiagnosis in Clinical Neurology*, 6th edition, (2012), 289–325. https://doi.org/10.1016/b978-1-4557-0308-1.00013-3
12. M. P. Pereira, S. Mühl, E. M. Pogatzki-Zahn, K. Agelopoulos, S. Ständer, Intraepidermal nerve fiber density: Diagnostic and therapeutic relevance in the management of chronic pruritus: A review, *Dermatol. Ther. (Heidelb)*, **6** (2016), 509–517. https://dx.doi.org/10.1007%2Fs13555-016-0146-1
13. S. Løseth, S. Lindal, E. Stålberg, S. I. Mellgren, Intraepidermal nerve fibre density, quantitative sensory testing and nerve conduction studies in a patient material with symptoms and signs of sensory polyneuropathy, *Eur. J. Neurol.*, **13** (2006), 105–111. https://doi.org/10.1111/j.1468-1331.2006.01232.x
14. M. Stefano, F. Cordella, S. M. L. Gioi, L. Zollo, Electrical stimulation of the human median nerve: A comparison between anatomical and simplified simulation models, in *10th International IEEE/EMBS Conference on Neural Engineering (NER)*, (2021), 769–772. https://doi.org/10.1109/NER49283.2021.9441187
15. J. H. K. Kim, J. B. Davidson, O. Röhrle, T. K. Soboleva, A. J. Pullan, Anatomically based lower limb nerve model for electrical stimulation, *Biomed. Eng. Online*, **6** (2007), https://doi.org/10.1186/1475-925X-6-48
16. M. Zelechowski, G. Valle, S. A. Raspopovic, A computational model to design neural interfaces for lower-limb sensory neuroprostheses, *J. NeuroEng. Rehabil.*, **17** (2020), https://doi.org/10.1186/s12984-020-00657-7
17. L. R. Humphrey, H. A. Hemami, A computational human model for exploring the role of the feet in balance, *J. Biomech.*, **43** (2010), 3199–3206. https://doi.org/10.1016/j.jbiomech.2010.07.021
18. J. W. Fernandez, M. Z. Ul Haque, P. J. Hunter, K. Mithraratne, Mechanics of the foot Part 1: a continuum framework for evaluating soft tissue stiffening in the pathologic foot, *Int. J. Numer. Methods Biomed. Eng.*, **28** (2012), 1056–1070. https://doi.org/10.1002/cnm.2494
19. K. Mithraratne, H. Ho, P. J. Hunter, J. W. Fernandez, Mechanics of the foot Part 2: A coupled solid-fluid model to investigate blood transport in the pathologic foot, *Int. J. Numer. Methods Biomed. Eng.*, **28** (2012), 1071–1081. https://doi.org/10.1002/cnm.2493
20. M. Z. Ul Haque, P. Du, L. K. Cheng, Geometrical interruption in the nerve anatomical model of the foot to simulate small fiber neuropathy, *Indian J. Sci. Technol.*, **10** (2017). https://dx.doi.org/10.17485/ijst/2017/v10i29/117372
21. M. Z. Ul Haque, P. Du, L. K. Cheng, A mathematical framework simulating nerve fibre physiology, *Int. J. Adv. Appl. Sci.*, **4** (2017), 124–129. https://doi.org/10.21833/ijaas.2017.010.017
22. A. L. Hodgkin, A. F. Huxley, A quantitative description of membrane current and its application to conduction and excitation in nerve, *J. Physiol.*, **117** (1952), 500–544. https://doi.org/10.1113/jphysiol.1952.sp004764
23. S. Y. Chiu, J. M. Ritchie, R. B. Rogart, D .Stagg, A quantitative description of membrane currents in rabbit myelinated nerve, *J. Physiol.*, **292** (1979), 149–166. https://doi.org/10.1113/jphysiol.1979.sp012843

24. C. H. Berthold, M. Rydmark, Morphology of normal peripheral axons, in *The Axon: Structure, Function and Pathophysiology*, Oxford University Press, New York, Oxford, (1995), 13–48. http://dx.doi.org/10.1093/acprof:oso/9780195082937.003.0002
25. H. Tohgi, H. Tsukagoshi, Y. Toyokura, Quantitative changes with age in normal sural nerves, *Acta Neuropathol.*, **38** (1977), 213–220. https://doi.org/10.1007/BF00688067
26. M. Z. Ul Haque, P. Du, L. K. Cheng, M. D. Jacobs, An anatomically-based model of the nerves in the human foot, *Int. J. Biomed. Biol. Eng.*, **6** (2012), 433–438. https://doi.org/10.5281/zenodo.1056751
27. M. Z. Ul Haque, P. Du, L. K. Cheng, M. D. Jacobs, An anatomically realistic geometrical model of the intra-epidermal nerves in the human foot, *IFMBE Proc.*, **43** (2014), 368–371. http://dx.doi.org/10.1007/978-3-319-02913-9_94
28. W. J. Hedley, M. R. Nelson, D. P. Bellivant, P. F. Nielsen, A short introduction to CellML, *Philos. Trans. R. Soc. London, Ser. A*, **359** (2001), 1073–1089. https://doi.org/10.1098/rsta.2001.0817
29. C. M. Lloyd, M. D. B. Halstead, P. F. Nielsen, CellML: its future, present and past, *Prog. Biophys. Mol. Biol.*, **85** (2004), 433–450. https://doi.org/10.1016/j.pbiomolbio.2004.01.004
30. J. Fernandez, P. Hunter, V. Shim, K. Mithraratne, A subject-specific framework to inform musculoskeletal modeling: Outcomes from the IUPS physiome project, In *Patient-Specific Computational Modeling*, *Lecture Notes in Computational Vision and Biomechanics*, Springer, Dordrecht, **5** (2012). https://doi.org/10.1007/978-94-007-4552-0_2
31. R. Ward, Electro-muscle stimulation therapy, *Compr. Biomed. Phys.*, **10** (2014), 231–253. https://doi.org/10.1016/B978-0-444-53632-7.01014-5
32. F. Yang, M. Anderson, S. He, K. Stephens, Y. Zheng, Z. Chen, et al., Differential expression of voltage-gated sodium channels in afferent neurons renders selective neural block by ionic direct current, *Sci. Adv.*, **4** (2018), eaaq1438. https://doi.org/10.1126/sciadv.aaq1438
33. H. J. Lee, J. R. Bach, J. A. Delisa, Deep peroneal sensory nerve: Standardization in nerve conduction study, *Am. J. Phys. Med. Rehabil.*, **69** (1990), 202–204. https://doi.org/10.1097/00002060-199008000-00006
34. N. Ongun, A. Oguzhanoglu, Comparison of the nerve conduction parameters in proximally and distally located muscles innervated by the bundles of median and ulnar nerves, *Med. Princ. Pract.*, **25** (2016), 466–471. https://doi.org/10.1159/000447742
35. S. J. Oh, Neuropathies of the foot, *Clin. Neurophysiol.*, **118** (2007), 954–980. https://doi.org/10.1016/j.clinph.2006.12.016
36. G. I. Wolfe, N. S. Baker, A. A. Amato, C. E. Jackson, S. P. Nations, D. S. Saperstein, et al., Chronic cryptogenic sensory polyneuropathy: clinical and laboratory characteristics, *Arch. Neurol.*, **56** (1999), 540–547. https://doi.org/10.1001/archneur.56.5.540
37. S. J. Oh, M. Demirci, B. Dajani, A. C. Melo, G. C. Claussen, Distal sensory nerve conduction of the superficial peroneal nerve: new method and its clinical application, *Muscle Nerve*, **24** (2001), 689–694. https://doi.org/10.1002/mus.1056
38. N. R. Holland, T. O. Crawford, P. Hauer, D. R. Cornblath, J. W. Griffin, J. C. McArthur, Small-fiber sensory neuropathies: clinical course and neuropathology of idiopathic cases, *Ann. Neurol.*, **44** (1998), 47–59. https://doi.org/10.1002/ana.410440111
39. D. Sene, Small fiber neuropathy: diagnosis, causes, and treatment, *Jt. Bone Spine*, **85** (2018), 553–559. https://doi.org/10.1016/j.jbspin.2017.11.002

40. P. Karlsson, A. M. Hincker, T. S. Jensen, R. Freeman, S. Haroutounian, Structural, functional, and symptom relations in painful distal symmetric polyneuropathies: a systematic review, *Pain*, **160** (2019), 286–297. https://doi.org/10.1097/j.pain.0000000000001381

AIMS Press